Coupled CFD-DEM Simulations for Modelling Non-Spherical Particles

Kiran MS[1], Rabijit Dutta[2], and Pritanshu Ranjan[1]

[1]Department of Mechanical Engineering, K K Birla Goa Campus, BITS Pilani, India
[2]Department of Mechanical & Nuclear Engineering, Virginia Commonwealth University, USA
kiran.ms44@gmail.com, rdutta@vcu.edu, pritanshur@goa.bits-pilani.ac.in

Abstract— **In the present work, single-spouted fluidized bed with non-spherical particle geometries was studied using Computational Fluid Dynamics–Discrete Element Modeling (CFD-DEM) coupling technique. CFD-DEM is an effective tool for modeling multi-phase flows in industrial applications such as fluidized bed reactors, spouted bed etc. Most DEM force-displacement models are based on particles with spherical geometry while many particles encountered in nature of non-spherical geometry. Three different shapes: Cylinder, Square and Hexagon were considered and the results are matched with the circular shaped particles. Multi-sphere method is used to model the force-displacement behavior. Open source software LIGGGHTS-DEM and OpenFOAM were used to perform the simulations. It was observed that the complex interactions of the multi-sphere particles give rise to greater instability in the fluidizing bed, as seen in strong fluctuations in particle properties. Also, these particles exhibited a tendency to agglomerate, thereby offering stronger resistance to shearing flows. As per the findings, it was concluded that the particle geometry has a significant influence on the performance of the fluidizing bed; failure to accurately represent an actual particle would result in erroneous results.**

Index Terms— **discrete element modeling, non-spherical particles, CFD-DEM coupling, turbulence modeling**

I. INTRODUCTION

Multiphase flows exist in many industrial applications such as gas or liquid fluidized bed reactors, fluidized bed dryers, spouted beds, three-phase gas-liquid-solid fluidized beds, pneumatic conveying of solids, and so on. A detailed knowledge of these flows is crucial for design, scale-up, optimization, and troubleshooting of such processes. Although this may be achieved by experimental techniques, modeling can be considered as an alternative tool for exploring different aspects of multiphase flows. The synchronization of Computational Fluid Dynamics (CFD) and Discrete Element Method (DEM) helps achieve this goal. CFD involves computation of the fluid-flow characteristics using the Navier-Stokes equation while DEM handles the interaction of solid particles with different phases i.e fluid,

wall, other solid particles using Newton's Laws of Motion. The coupling between these two disciplines is modeled via the interaction forces existing between the phases on account of Newton's Third Law. Selection of the appropriate CFD Turbulence Model and DEM Force Displacement Models, Contact Search Algorithm, Integration Methods is of paramount importance in order to minimize errors, reduce computational time and efficient utilization of memory. Another key parameter in CFD-DEM simulations is the shape representation of the solid particles. Most Force Displacement models are formulated using the soft-sphere or hard-sphere approach where the solid particles are assumed to be spherical in shape. However, many applications in industry and medicine involve non-spherical particles whose rigid body dynamics vary considerably from that of spherical particles. In addition, dynamics of non-spherical particles is dependent upon particle orientation; rotation about center of mass, interlocks between particles etc. which do not apply to spherical particles. CFD-DEM simulation of non-spherical particles is an active field of research, open to novel techniques and improvements. Several studies have been conducted with regard to Force-Displacement Models, Contact Search Algorithms etc. The work of Kloss, C. et al. [1] provides a comprehensive overview of CFD-DEM approach based on the open-source software packages OpenFOAM and LIGGGHTS. Zhong et al. [2] conducted an extensive literature review of theoretical developments and applications of DEM Modeling in NSPS (Non-Spherical Particulate Systems). Zhou et al. [3] developed a novel CFD-DEM model by coupling two software OpenFOAM and PFC and the reliability of this model was demonstrated in the case of soil erosion and bridge scour problems. They also conducted experimental studies and transient CFD-DEM simulations in a fluidized bed employing different drag models. Studies conducted by [4] involved coupling a two-equation turbulent model for gas motion and a DEM Model to simulate gas-solid turbulent flow in a cylindrical spouted bed with a conical base. The work was further extended to simulate the flow using corn-shaped multi-sphere particles [5]. Similarly, Farivar et al. [6] studied the simulation of fluidization of cylindrical particles in a fluidized bed.

LIGGGHTS-DEM is commonly used open-source software for Discrete Element Method. However, the

---

public version of LIGGGHTS is designed to handle only spherical particles. The aim of this work is to extend the existing LIGGGHTS-PUBLIC code to simulate 3D solid-particle flows using multi-sphere particles. Firstly, the flow across an 180^0 Square Bend was analyzed using different turbulence models and the corresponding results were compared with the experimental data to determine the most accurate model. The purpose of this study was to validate CFD predictions. Later, studies were carried out on a single-spout fluidized bed using coupled OpenFOAM-LIGGGHTS, initially employing spherical particles for validating against existing literature, followed by custom-made multi-sphere particles. A comparative analysis of the parameters in the two cases demonstrates the effect of particle-shape on the outcome of the simulations.

II. CFD VALIDATION

Before discussing the DEM formultaion it is important to validate the CFD software OpenFOAM which will be used to carry out the flow simulations. To validate OpenFOAM CFD results an 180^0 square cross-sectional bend was chosen as shown in Fig. 1. Hexahedral meshing was done to capture the flow physics. The bend gives rise to strong secondary flows which produce a very complex cross-stream flow distribution with a pronounced trough in velocity near the inside of the bend. Accurate prediction of these troughs is a suitable test for flow prediction capabilities. Two turbulence model was tested, *STD k-ε* and *SST k-ω*, were tested for flow prediction. Pressure velocity coupling was achived using Pressure-Implicit with Splitting of Operators (PISO) algorithm. Central differencing was used to dicretize laplacian terms and second order upwind scheme for discretizing the divergence term. Convergence criterion was set as 10^{-6} for all the variables to achieve accurate results.

The velocity profiles detailed in Iacovides H et al. [8] were used for validation. Out of the various profiles available in [8], cross-stream velocity profiles (ranging from inner to outer bend) at a height of z/D=0.5 (z is the

cross-stream height and D is the diameter of the pipe) and $\Phi = 45^0, 90^0$ and 135^0 were compared with the profiles obtained from the simulation and are shown in Fig. 2. From Fig. 2, it was noticed that the profiles obtained from the *SST k-ω* model showed relatively better agreement with the experimental data as compared to those obtained by the *STD k-ε* model. It was noted that at Bend Angle= 45^0, the cross-stream velocity profiles obtained from the two models are similar, but as the secondary flows become more prominent, there is noticeable difference in the profiles. It was also noted that for any bend angle, the flow profiles are similar in the core region, but significantly differ near the wall. Henceforth, all simulations were performed using the *SST k-ω* Model.

(a)

(b)
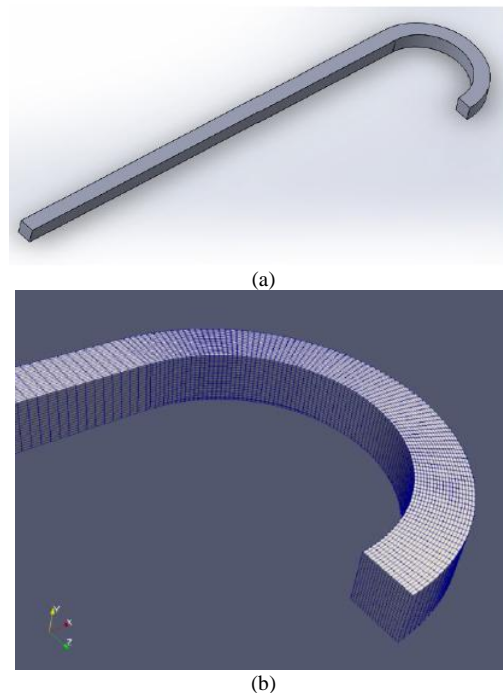
Figure 1.   (a) Square Bend geometry with cross section 88.9X88.9mm, (b) Square Bend mesh created on ANSYS ICEM
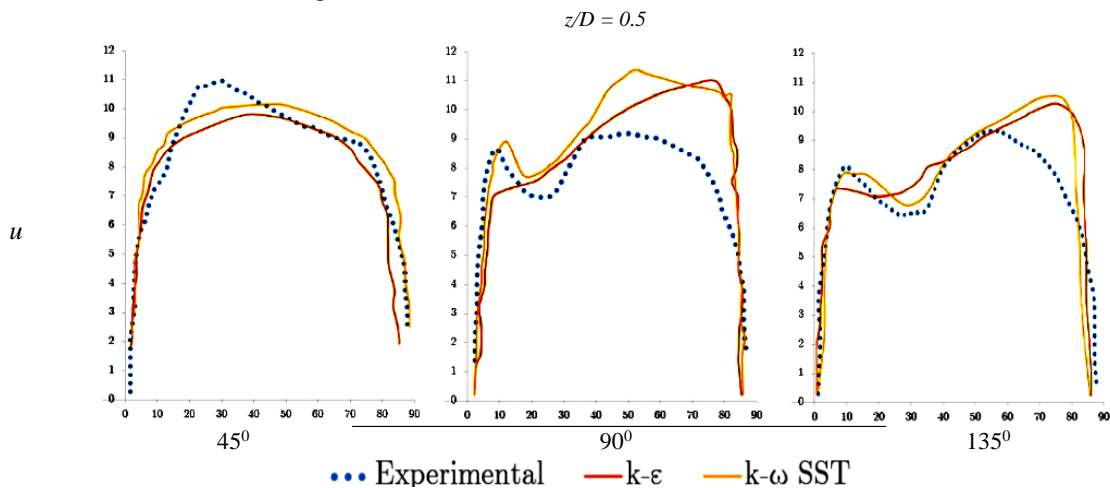
Figure 2.   Comparison of cross-stream velocity profiles obtained from *STD k-ε* and *SST k-ω* models with the experimental velocity profiles of [8]. The profiles go from inner(left) to outer(right)

III. DEM FORMULATION

Force-displacement models are used to calculate collision properties as a function of normal and tangential overlaps, physical properties and collision history of colliding particles. The model used in this study is the non-linear Mindlin and Deresiewicz Model based on the Hertz classical theory of contact mechanics. The nonlinear viscoelastic contact force model consists of two components, elastic and viscous forces. The elastic force is calculated by Hooke's Law and conserves the kinetic energy of the collision while the viscous force dissipates the kinetic energy. The normal component of the collision force is given:

$$f_{ij}^n = f_{el}^n + f_{diss}^n = -(k_n\delta_n)n_{ij} - (\eta_n v_{rn})n_{ij} \quad (1)$$

$$v_{rn} = v_{ij}.n_{ij} \quad (2)$$

The axisymmetric normal pressure $P(r)$ is integrated, as shown in Fig. 3 to obtain the resultant normal force F_L, which gives the normal deformation as:

$$\delta_n = \frac{a^2}{R_{eff}} = \left(\frac{9}{16}\frac{F_L^2}{R_{eff}E_{eff}^2}\right)^{\frac{1}{3}} \quad (3)$$

Similarly, the tangential component of the collision force is given by:

$$f_{ij}^t = f_{el}^t = -8G_{eff}\sqrt{R_{eff}}\delta_n^{\frac{1}{2}}\delta_t t_{ij} \quad (4)$$

The torque is then calculated using the Spring-Dashpot Model.

(a)   (b)
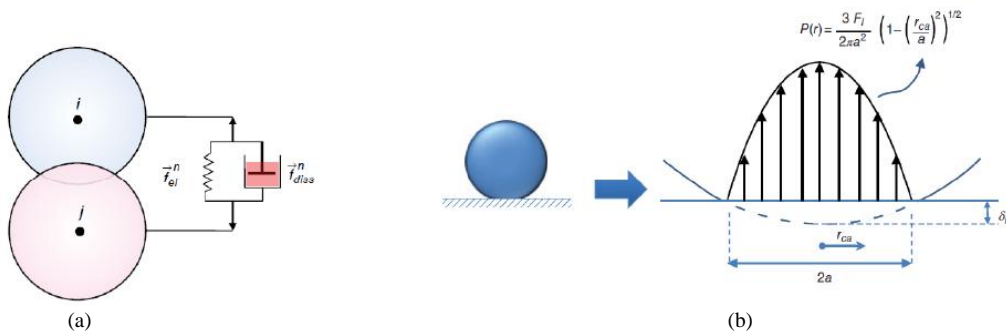
Figure 3. (a) represents the visco-elastic model. (b) represents the normal pressure distribution in the contact area of an elastic sphere as a function of contact radius

(a)   (b)   (c)   (d)
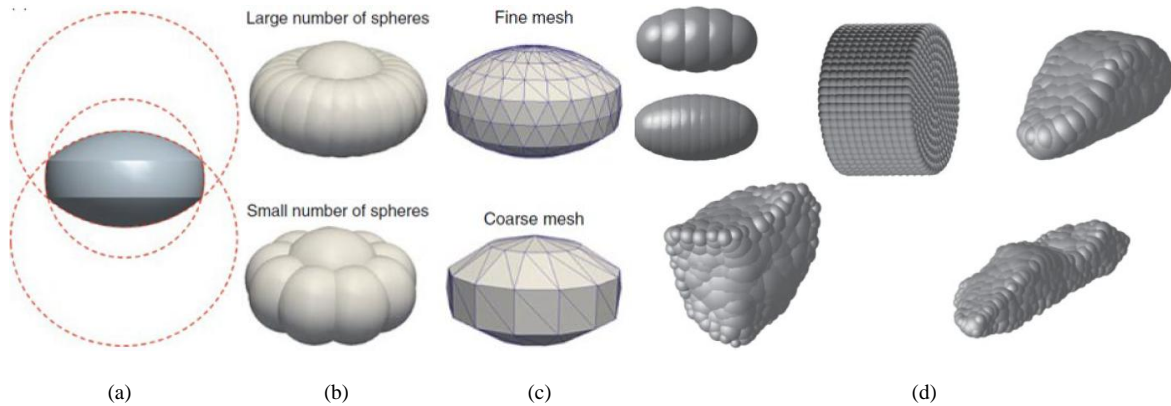
Figure 4. (a) Method of intersecting surfaces, (b) Multi-sphere method, (c) Polyhedral method, (d) A wide variety of shapes can be approximated using the multi-sphere method

For non-spherical particles, there are multiple ways of generating these particles in the simulation domain. In the present framework multi-spheres method is used to generate these particles. Fig. 4 shows different methods for generating non-spherical particles. It can be seen from Fig. 4(b) that increasing he number of sphere to create the particle increases the smoothness and accuracy of the particle but it will require more computaional resources.
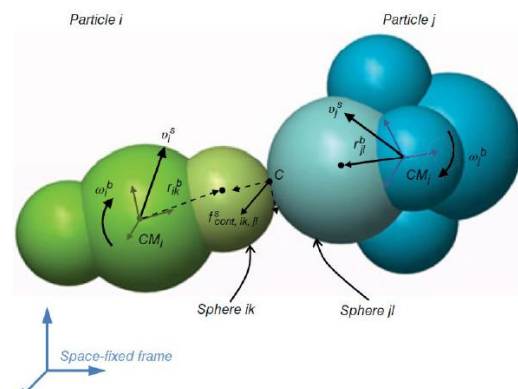
Figure 5. Interaction between multi-sphere particles.

The reason for using the multi-sphere method is that all the force-displacement models, contact search algorithms etc. derived for spherical particles can be easily extended to multi-sphere particles with a few modifications to the calculation of force. Also, these formulations are universal and require no further modifications from shape to shape. Fig. 5 shows that the interaction between multi-sphere particles depends only on the interaction of their constituent spheres in contact. These factors make the multi-sphere method most favorable for the current work.

Norouzi et al. [9] conducted a vertical free fall test of a single-sphere and a multi-sphere particle, generated using the same sphere, under similar conditions. The two particles followed the path as depicted in Fig. 6. The coefficient of restitution was found to be 0.8 and 0.95 respectively. This difference may be attributed to the way in which the normal damping coefficient is calculated. The damping coefficient is given by:

$$\eta_n = \frac{-2 \ln e_n \sqrt{m_{eff} k_n}}{\sqrt{(\ln e_n)^2 + \pi^2}} \qquad (5)$$

The coefficient of restitution is related to the square root of mass. When the damping coefficient of a single sphere is applied to the spheres in the multi-sphere particle, the effect of total mass on restitution coefficient is not taken into account. Therefore, the damping coefficient in the multisphere should be adjusted to obtain a correct coefficient of restitution.
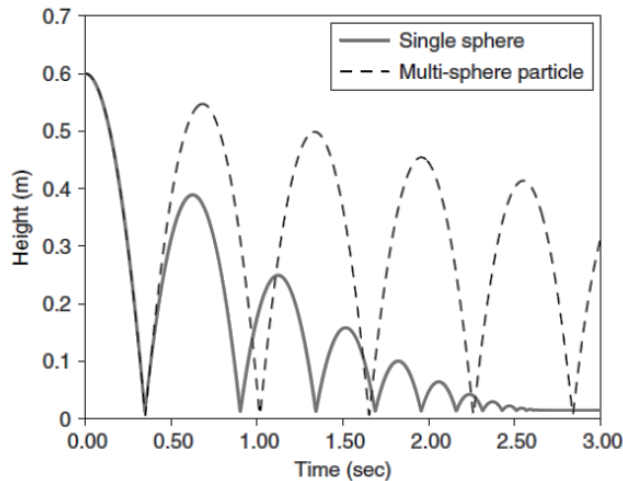
Figure 6. The evolution of height of particle in free fall tests with single-sphere and multi-sphere particles. Spheres in the multi-sphere particle are identical to sphere used in the single-sphere free fall. Courtesy: Norouzi et al. [9]

For CFD-DEM coupling between solid phase at particle scale and fluid phase at fluid cell scale is done via drag force and with empirical or theoretical correlations developed for the flow across a single particle or an assembly of particles. Also, an average force is employed. In the present study, the mesh has been generated such that average fluid cell is bigger than the particles, as shown in Fig. 7. The solid phase information is available at the particle scale while the fluid phase information is available at the fluid cell scale Δx. Therefore, special attention is required when particle scale information is used to calculate a fluid cell property and vice versa. This approach employs volume averaging of the granular phase properties, the size of the fluid cells must be sufficiently larger than the solid particles to obtain a proper average representation. Though a fine mesh is generally preferred, the void fraction field may become discontinuous if the cells are too small, thereby impairing numerical stability.
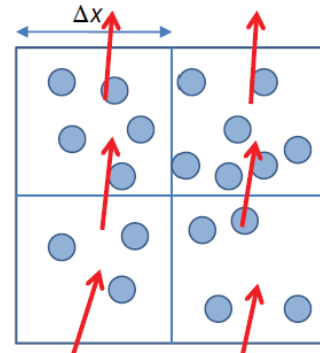
Figure 7. Solid and Fluid Cell configuration for the present case.

IV. RESULTS AND DISCUSSION

In the present section validation of CFD-DEM application is discussed and then the effect of different shaped particles will be discussed for a fluidized bed.

A. Validation of CFD-DEM

Spouted bed is a cyclic gas-solid system, in which high momentum spouting gas entering from the central spout rapidly carries the particles, following which these particles rain back into the annulus region between the spout and the wall. Then, under the influence of the background fluidisation air, they slowly travel downward and inward as a loosely packed bed. The geometry for the single-spout fluidized bed was based on the work of [3]. The bed dimensions are 145mm x 20mm x 1000mm with two sets of inlets: the central strip of 5mm width is the spout inlet; the adjacent inlets each of 70mm width are for the background fluidisation air, as shown in Fig. 8(a). Gravity acts in the negative z-direction. The hexahedral mesh generated on ANSYS ICEM has a total of 6460 elements and 5130 nodes, Fig. 8 (b).
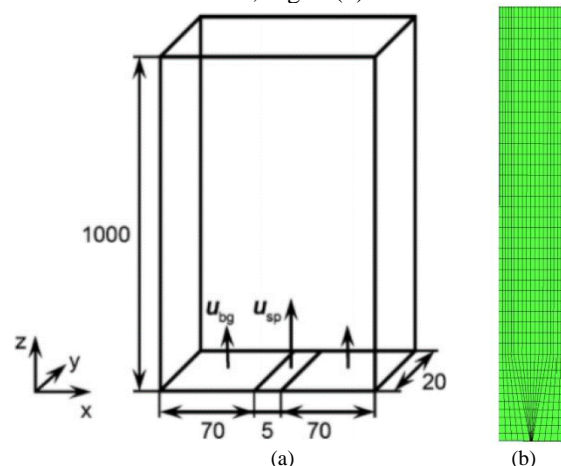
Figure 8. (a) Geometry of the single-spout fluidized bed, (b) Hexahedral mesh

The boundary conditions used were similar to those used in van Bujitnen et al. The inlet velocity at the spout U_{sp} was 43.5 m/s while the velocity of the background fluidisation air U_{bg} was 2.4 m/s. A pressure outlet condition was used at the outlet. CFD-DEM simulations using different multi-sphere particles were conducted, namely spherical, square, cylindrical and hexagonal. The other 3 particles were constructed using the spherical particle as the base unit. The radius of the spherical unit was 1.5mm, while the radius of the contact sphere surrounding the spherical/multi-sphere particle was set to 4mm. In order to incorporate custom-made multi-sphere particles into the simulation, a data file was provided as part of the initializing parameters. This data file contains the spatial coordinates and the radius of each sphere that is a constituent of the particle. LIGGGHTS ensures that the relative position between the spheres does not change in order to maintain the multi-sphere shape. For the validation simulation using spherical particles, a total of 12000 particles were used while 7200 particles were used in the comparative analyses with the other geometries. The hexagon simulation consisted of 1200 particles (7200 spheres in total), cylinder and square simulations both consisted of 1800 particles (7200 spheres). Limited computational facilities prevented the use of more than 7200 spheres.

TABLE I. MATERIAL PROPERTY AND SIMULATION SETTINGS

Young's Modulus	1E7 N/m^2
Gas Density	1.205 kg/m^3
Particle Density	2505 kg/m^3
Poisson's Ratio	0.45
Coefficient of Restitution a) Spherical b) Cylindrical c) Square d) Hexagon	 0.1 0.5 0.5 0.59
Coefficient of Friction	0.3
CFD Time Step	5E-4
DEM Time Step	1E-5
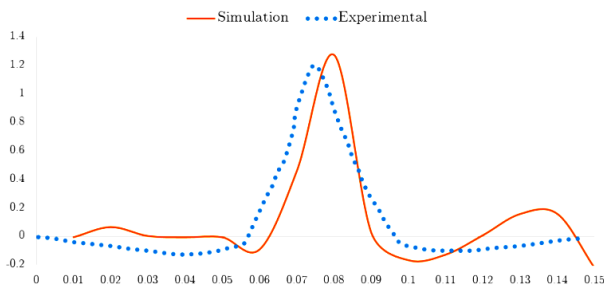
Figure 9. Plot of Average Particle z-velocity V/s x-position at a plane z=0.05m, present result vs. experimental result [3]

Table I shows the material property and time step used for CFD-DEM simulations. The validation, as shown in Fig. 9, was done against the experimental results of [3] by plotting average particle z-velocity V/s x-position for spherical particles. The first simulation was run with a

relatively coarser mesh with 3640 nodes and 4218 elements, giving a peak average Z-velocity of 2.2 m/s. The mesh was gradually refined, particularly the core region. The peak average value gradually converged from 2.2 to 1.5 and finally 1.27 m/s, which is in close agreement with the experimental value of 1.2 m/s. The final mesh consisted of a total of 6460 elements and 5130 nodes. The simulation time was 5 minutes 11 seconds. Hence the results were validated and the existing CFD-DEM setup was utilized for the next set of simulations.

Using the same setup i.e. boundary conditions, mesh and simulation time steps and duration, simulations were run using the other particle geometries namely hexagon, cylinder and square. Due to difference in their rigid body dynamics, a considerable difference was noticed in the average z-velocity v/s x-position plot. From the computational point of view, each simulation had a different runtime.
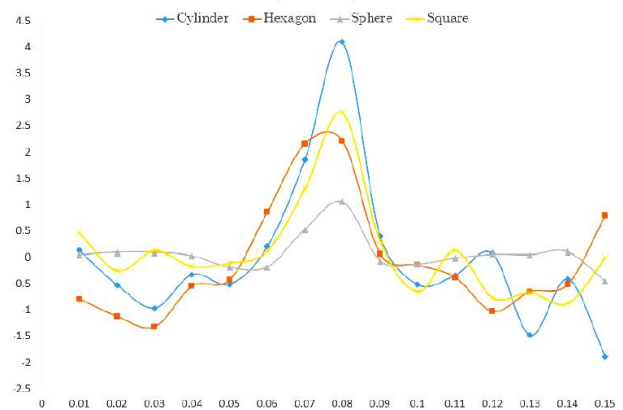
Figure 10. Comparison average particle z-velocity vs x-position at z = 0.05 m for different particle geometries at z = 0.05m.

From Fig. 10 it can be observed that the peak average velocity for the spherical particles was 1.04 m/s as compared to 1.27 m/s of the previous case. This is due to the reduction in the number of particles used, implying lesser particles at the core region therefore statistically reducing the peak value. The spherical particles show a smooth trend in z-velocity values across the x-length, with one maxima in the core region. The non-spherical particles exhibit stronger fluctuations in average Z-velocity as well as higher peak values in comparison to the sphere. The peak average velocities of the square, hexagon and cylinder are 2.2 m/s, 2.7 m/s and 4.1 m/s respectively.

These particles experience greater drag force by the incoming flow due to greater projected area, thereby resulting in higher momentum imparted by the flow. The non-spherical nature is characterized by increasingly stronger interactions such as collision, friction and interlocking, as well as a non-zero lift force that varies with particle orientation. This causes increasing instabilities of spouting in the bed, as seen by the strong fluctuations in the average z-velocity values. Each multi-sphere particle is 4-6 times heavier than its constituent sphere. Considering the low-momentum background fluidization air, the non-spherical particles travel down with a much greater velocity in comparison with

spherical particle, as seen in Fig. 10. Out of the 4 geometries, the cylinder possesses the greatest moment of inertia, thereby resulting in greater torque and stronger collisions. As seen in Fig. 10, the cylinder exhibits the greatest fluctuations in average Z-velocity values. Further particle distribution is plotted four different time frames and is shown in Fig. 11. As seen in Fig. 11, the spherical particles are widely distributed across the height of the fluidizing bed as the simulation time increases as compared to non-spherical particles. The least distribution is seen for the cylindrical particle, Fig. 11 (d).

At the initial time, Fig. 11 (a,b), it can be seen that non-spherical particles experiences immediate effect of fluidization air momentum and starts to distribute in Y-direction. The non-spherical particles have a tendency to either produce dilute packing fractions or agglomerate due to interlocking, resulting in the solid-like assemblies. The assemblies or clusters show a stronger resistance to the shearing flows than smooth spheres, which will hamper the performance of the fluidizing bed. As seen in Fig. 11(d), these clusters are found at the extreme ends of the bed height.

(a)   (b)

(c)   (d)

Figure 11. The screenshots of the solid-particle flow in the single-spout fluidized bed dryer using different particles from left to right: Spherical, Cylinder, Square, Hexagon. Out of a total of 18 timeframes, the following are at a) Time-frame 1, b) Time-frame 2, b) Time-frame 5, b) Time-frame 18

V. CONCLUISIONS

The study focused on the coupled CFD-DEM simulations of non-spherical particles using OpenFOAM and LIGGGHTS. The existing LIGGGHTS-PUBLIC code, initially programmed to handle only spherical particles, was modified to enable multi-sphere CFD-DEM simulations. Effect of particle geometry was studied for a spouted bed. Three shapes were considered: square, cylinder and hexagon. The average particle Z-velocity V/s X-Position at Z=50mm was plotted for all four geometries. The spherical particle showed a smoother trend across the bed length while the multi-sphere particles showed greater fluctuation in values. The rotation of these particles results in stronger collisions while the non-spherical nature gives rise to additional lift forces which do not occur in the case of spherical particles. Also, these particles exhibited a tendency to agglomerate and form solid-like assemblies, which

hindered the bed performance by strongly resisting the shearing flows. Particle geometry also had a considerable influence on the simulation time.

CONFLICT OF INTEREST

The authors declare no conflict of interest.

AUTHOR CONTRIBUTIONS

Kiran MS conducted the research and analyzed the results; Rabijit Dutta was involved into conceptualization and writing the paper; Pritanshu Ranjan wrote the paper; all authors had approved the final version.

REFERENCES

[1] C. Kloss, C. Goniva, A. Hager, S. Amberger, and S. Pirker, "Models, algorithms and validation for open source DEM and CFD-DEM, " *Progress in Computational Fluid Dynamics*, Vol. 12, Nos. 2/3, pp.140–152, 2012.

[2] W. Zhong, A. Yu, X. Liu, Z. Tong, and H. Zhang, "DEM/CFD-DEM modelling of non spherical particulate systems: Theoretical developments and applications," *Powder Technology*, vol. 302, pp. 108-152, 2016.

[3] H. Zhou, G. Wang, C. Jia, C. Li, "A Novel, coupled CFD-DEM model for the flow characteristics of particles inside a pipe," *Water*, vol. 11, no. 11, p. 2381, 2019.

[4] B. Ren, W. Zhong, B. Jin, Z. Yuan, Y. Lu, "Computational Fluid Dynamics (CFD)–Discrete Element Method (DEM) simulation of gas–solid turbulent flow in a cylindrical spouted bed with a conical base," *Energy & Fuels*, vol. 25, no. 9, pp. 4095-4105, 2011.

[5] B. Ren, W. Zhong, Y. Chen, X. Chen, B. Jin, Z. Yuan, Y. Lu, "CFD-DEM simulation of spouting of corn-shaped particles," *Particuology*, vol. 10, no. 5, pp. 562–572, 2012.

[6] F. Farivar, H. Zhang, Z. F. Tian, and A. Gupte, "CFD-DEM simulation of fluidization of ulti-sphere-modelled cylindrical particles," *Powder Technology*, 2019.

[7] V. Srinivasan. CFD – DEM Modeling and Parallel Implementation of Three Dimensional Non- Spherical Particulate Systems. Retrieved 11 October 2020, [Online]. Available: http://hdl.handle.net/10919/91889, 2020.

[8] H. Iacovides, B. Launder, P. Loizou, H. Zhao, "Turbulent boundary-layer development around a square-sectioned U-bend: Measurements and computation, " *Journal of Fluids Engineering*, vol. 112, no. 4, pp. 409-415, 1990

[9] H. Norouzi, R. Zarghami, R. Sotudeh-Gharebagh, N. Mostoufi, *Coupled CFD-DEM Modeling: Formulation, Implementation and Application to Multiphase Flows,* John Wiley & Sons, 2016.

[10] H. Versteeg and W Malalasekera, *An Introduction to Computational Fluid Dynamics*. Pearson Pranctice Hall, 2nd Edition, 2007.

[11] X. Liu, J. Gan, W. Zhong, A. Yu, "Particle shape effects on dynamic behaviors in a spouted bed: CFD-DEM study," *Powder Technology*, 2019.

Kiran MS was born in Bengaluru, Karnataka, India. He did is Bachelor's degrees in Mechanical engineering from BITS Pilani, India in 2021. He is currently pursuing His Masters in Computational and Data-Driven Engineering from Columbia University. He has worked in predominantly in the area of Computational Fluid Dynamics and currently working in the usage of Neural Network in engineering areas.

Rabijit Dutta was born in Assam, India. He did his Bachelor's degrees in Mechanical engineering from Department of Mechanical Engineering, Jorhat Engineering College, Assam, India in 2006. He completed his Masters and PhD from Department of Applied Mechanics, IIT Delhi in the year 2009 and 2014 respectively. His primary research interest lies in understanding industrial and biological transport phenomena using high-fidelity numerical computations. He has worked in the area of turbulence modeling for jet impinging flows and boundary layers in roughened turbine blades and the development of verification and validation methods for large eddy simulation. He is currently working as a Post-Doctoral Fellow in Virginia Commonwealth University in the Department of Mechanical & Nuclear Engineering.

Pritanshu Ranjan was born in Varanasi, India. He did his Bachelor's degrees in Mechanical engineering from Department of Mechanical Engineering, GJUS&T Hisar, Haryana, India in 2008. He completed his PhD from Department of Applied Mechanics, IIT Delhi in the year 2017. His primary research interest lies in Turbulence Modeling, Partially Averaged Navier-Stokes method, Large Eddy Simulation, Flow control technique in adverse pressure gradient flow field and Mixed convection in turbulent channel flows and heat transfer enhancement. He is currently employed as an Assistant Professor in Department of Mechanical Engineering in Goa Campus of BITS Pilani, India.